Thermoelectric and magnetotransport properties of $Bi_{1-x}Sb_x$ thin films and Bi/CdTe superlattices

1999 J. Phys.: Condens. Matter 11 5157

(http://iopscience.iop.org/0953-8984/11/26/316)

J. Phys.: Condens. Matter **11** (1999) 5157–5167. Printed in the UK PII: S0953-8984(99)00924-8

Thermoelectric and magnetotransport properties of $Bi_{1-x}Sb_x$ thin films and Bi/CdTe superlattices

I Vurgaftman†, J R Meyer†, C A Hoffman†, S Cho‡, A DiVenere‡, G K Wong‡ and J B Ketterson‡

† Code 5600, Naval Research Laboratory, Washington, DC 20375, USA
‡ Department of Physics, Northwestern University, Evanston, IL 60208, USA

Received 13 January 1999

Abstract. The magnetotransport properties of $Bi_{1-x}Sb_x$ thin films ($x = 0$, 0.09 and 0.16) and Bi/CdTe superlattices have been determined by applying the quantitative mobility spectrum analysis (QMSA) and multicarrier fitting to the magnetic-field-dependent resistivities and Hall coefficients, using algorithms which account for the strong anisotropy of the mobilities. The experimentally derived electron and hole densities and mobilities are then used as the input to a nonparabolic and anisotropic band model that derives the thermal occupations and relaxation times for L-valley electrons and holes as well as T-valley and H-valley holes. This allows a calculation of the thermoelectric properties for comparison with experimental results. While the data for a Bi thin film and Bi/CdTe superlattices are reproduced quite well without any adjustable parameters, for $Bi_{1-x}Sb_x$ thin films a non-uniform doping profile must be assumed.

1. Introduction

Interest in the Bi–Sb material system has recently been stimulated by the promise of a new generation of thermoelectric materials based on alloyed and reduced-dimensionality structures [1–6]. Although elemental bismuth and antimony are both semimetals, the $Bi_{1-x}Sb_x$ alloy is a semiconductor in the composition range $0.07 < x < 0.22$ [4], which is capable of yielding a significantly higher thermopower at low temperatures [7]. Furthermore, the inducement of a semimetal-to-semiconductor transition by quantum confinement in Bi-based superlattices [2] with Bi wells thinner than ≈300 Å may potentially lead to high thermoelectric figures of merit at room temperature and above. H-point holes with a sixfold valley degeneracy may produce high p-type thermopowers, and strain effects in strain-compensated $Bi_{1-x}Sb_x$-based heterostructures could provide further enhancements.

In spite of the technological potential of Bi-based thin films and superlattices, many of the relevant properties of these structures remain relatively unexplored. In this article, we will discuss a detailed model for the thermoelectric properties of BiSb-based heterostructures which self-consistently incorporates the field-dependent Hall and resistivity data. The quantitative mobility spectrum analysis (QMSA) [8], which derives multiple electron and hole densities and mobilities from the magnetotransport measurements, has been modified to account for the strong anisotropy of the electrical conduction in these materials. We will show that the experimental thermopowers can be accounted for in detail. The potential for using the transport/thermopower data to extract band parameters will also be examined.

0953-8984/99/265157+11$19.50

2. Experiment

The growth of Bi thin films, BiSb thin films and Bi/CdTe superlattices on semi-insulating (111)B CdTe substrates by molecular beam epitaxy has been described in detail elsewhere [9, 10]. The following specimens grown by these methods will be treated in the present study. The Bi thin film was 0.5 μm thick, while the $Bi_{1-x}Sb_x$ films with $x = 0.09$ and $x = 0.16$ were 1 μm thick. Two Bi/CdTe superlattices with 400 Å/100 Å (nine periods) and 800 Å/100 Å (five periods) well/barrier thicknesses were also grown. CdTe is eminently suitable as a barrier for superlattice thermoelectric devices owing to its near lattice match with Bi, large energy gap and low thermal conductivity. In all cases, the growth direction was parallel to the trigonal axis of the Bi-based materials, which have a rhombohedral crystal structure that is distorted from cubic symmetry.

The resistivities and Hall coefficients of all structures were measured as a function of magnetic field ($0 \leqslant B \leqslant 7$ T) and temperature ($4.2 < T < 300$ K) by the van der Pauw technique, with current flow in the plane perpendicular to the trigonal axis.

For the thermoelectric characterization, samples were processed into bar-shaped patterns using photolithography and lift-off techniques. A differential method was employed, in which a small temperature difference was maintained across the sample to produce the thermoelectric voltage: $\Delta V = S\nabla T + b(\nabla T)^2 + \cdots$, where b is a constant. The thermoelectric voltage, $(\Delta V)_i$, against temperature difference values, $(\Delta T)_i$, were then plotted, and the thermopower determined from the slope of the linear region. To measure the temperature difference across the sample, we used a differential Cu–constantan thermocouple. The thermoelectric voltage was measured by using thin copper leads and was later corrected for the thermopower of the leads to obtain the final results [3].

3. Anisotropic magnetotransport analysis

The magnetotransport results were analysed using a quantitative mobility spectrum analysis (QMSA) procedure [11, 12], which derives carrier densities and mobilities for all of the species present. A number of important improvements [13] were recently incorporated into QMSA, which now offers a better overall extraction of information from experimental data sets than any previous technique.

In order to treat materials such as Bi and Sb (as well as n-type Si, Si-Ge, SiC, AlAs and lead salts), in which carriers in the L, X and H valleys have distinct effective masses and hence different mobilities along at least two of the symmetry axes, the expressions for the conductivity tensor components used in QMSA must be modified to have the following forms:

$$\sigma_{xx}(B) = \sum_{i=1}^{N} n_i e \left[\frac{C(\mu_{i1} + \mu_{i2})}{2(1 + \mu_{i1}\mu_{i2}B^2)} + \frac{(1-C)\mu_{i1}}{1 + (\mu_{i1}B)^2} \right] \tag{1}$$

$$\sigma_{xy}(B) = \sum_{i=1}^{N} s_i n_i e \left[\frac{C\mu_{i1}\mu_{i2}B}{1 + \mu_{i1}\mu_{i2}B^2} + \frac{(1-C)\mu_{i1}^2 B}{1 + (\mu_{i1}B)^2} \right] \tag{2}$$

where the sum is over carrier species, n_i is the density for a given species, μ_{i1} and μ_{i2} are the distinct mobilities along the two in-plane axes and s_i is +1 for holes and -1 for electrons. Although $C = 2/3$ for most X-valley and L-valley systems, $C = 1$ in the special case of L-valley carriers in Bi and BiSb with transport perpendicular to the trigonal axis, since all three L valleys have their symmetry axes in the same plane [14]. Note that the T-valley holes in Bi and BiSb are isotropic in the plane ($\mu_{i1} = \mu_{i2}$).

As in the isotropic QMSA, the discrete carrier species i are replaced by a fine grid, which represents the mobility spectrum [15]. The QMSA approach determines which combination of carrier type and mobility will produce the greatest reduction in the errors in the magnitudes and slopes of the conductivity tensor components. Empirical mobility spectrum manipulation procedures are also employed to improve the quality of the fits while at the same time making the spectra smoother and more physically reasonable. The details of the anisotropic QMSA procedure have been presented elsewhere [8].

4. Modelling of the carrier statistics, transport and thermopower

The non-parabolic and anisotropic dispersion relations for the L-valley, T-valley and H-valley carriers are taken from the Lax model [16]:

$$\varepsilon(k) = \pm\tfrac{1}{2}(\varepsilon_g^2 + 2\varepsilon_g\hbar^2 m_0^{-1}\boldsymbol{k}\mathbf{m}^{-1}\boldsymbol{k})^{1/2} - \tfrac{1}{2}\varepsilon_g \tag{3}$$

where ε_g is the energy gap at the L, T or H point, $\boldsymbol{k}$ is the electron wavevector and $\mathbf{m}^{-1}$ is the nondiagonal reciprocal effective mass tensor at the band extremum [1]. Using these dispersion relations, equilibrium electron and hole Fermi energies were calculated with carrier densities derived from analysis of the field-dependent magnetotransport data. Energy gaps and effective masses for each alloy composition were taken from the literature [16], with best estimates made concerning the temperature dependence of each energy gap. The numerical values of the various parameters are specified in table 1.

Table 1. Energy gaps and effective masses for $Bi_{1-x}Sb_x$ in several relevant valleys. The T-valley parameters are assumed to be the same in Bi and BiSb, and the H-valley masses are taken to be equal to those in Sb. For definitions of the mass tensor components, see [1]; the rest of the references are as indicated.

	L	T	H
E_g (meV)	$13.6 - 272.5x + 0.002T + 0.075T^2$ [4, 26]	407.5 [27]	—
m_1/m_0	$0.0014E_g/E_g(x=0,T=0)$ [31]	0.059 [31]	0.068 [16]
m_2/m_0	$0.291E_g/E_g(x=0,T=0)$ [31]	0.059 [31]	0.92 [16]
m_3/m_0	$0.0071E_g/E_g(x=0,T=0)$ [31]	0.634 [31]	0.05 [16]
m_4/m_0	$0.0359E_g/E_g(x=0,T=0)$ [31]	0	0

To model the thermopower in the Bi thin-film and superlattice samples, we need to account for various carrier scattering mechanisms. Intravalley acoustic phonon scattering and electron–hole interband intervalley scattering by short-wavelength phonons are the most important processes in semimetallic Bi [17, 18]. For the present films, we also include boundary roughness scattering, which can limit the mobility at low temperatures [19]. The electron and hole in-plane conductivities and mobilities are then calculated taking into account the off-diagonal elements of the reciprocal mass tensor. The absolute magnitudes of the energy-dependent relaxation times for both electrons and holes have been normalized by fitting the experimental QMSA and multicarrier mobilities for each carrier species.

The thermopower for a given valley i is finally calculated using the relation [20]

$$S_i = k_B\left(\frac{\langle\varepsilon\tau_i(\varepsilon)/k_BT\rangle}{\langle\tau_i(\varepsilon)\rangle} - \frac{E_{Fi}}{k_BT}\right) \tag{4}$$

where $\tau_i(\varepsilon)$ is the energy-dependent momentum relaxation time, E_{Fi} is the Fermi level and the brackets represent a statistical average that is weighted by the product of the Fermi distribution function and its complement $[f_{0i}(1-f_{0i})]$. The net thermopower is averaged over all electron and hole species with appreciable concentrations:

$$S = \frac{\sum_i S_i n_i \mu_i}{\sum_i n_i \mu_i}. \tag{5}$$

Since the electron and hole contributions have different signs, the thermal generation of minority carriers in zero-gap and narrow-gap systems can produce a significant reduction of the thermopower.

While QMSA nearly always provides reliable results, the data for the $Bi_{0.91}Sb_{0.09}$ and $Bi_{0.84}Sb_{0.16}$ films were especially noisy at magnetic fields <0.5 T, due in part to the low sample resistance and material nonuniformities. The remaining data showed insufficient sensitivity to allow an independent extraction of the densities and mobilities for all carrier species from QMSA. For those samples, we therefore carried out a more conventional multicarrier fit [21], using equations (1) and (2) in conjunction with the constraint that the net doping density $(n-p)$ remain constant for all temperatures.

5. Results

5.1. Bi thin film

We first consider the Bi thin film, which is taken to be semimetallic with a 38 meV overlap between the conduction band minima in the L valleys and the valence band maximum in the T valley [16]. In QMSA the holes are therefore assumed to be isotropic, whereas a large mobility ratio of $\mu_{i2}/\mu_{i1} = 60$ is employed for the anisotropic electrons residing in the L valleys [22, 23]. QMSA results for the carrier densities and mobilities as a function of temperature are shown in figures 1 and 2, respectively. The results for the carrier concentrations are in good agreement with those of previous investigations of bulk Bi samples [24] and with the densities predicted by

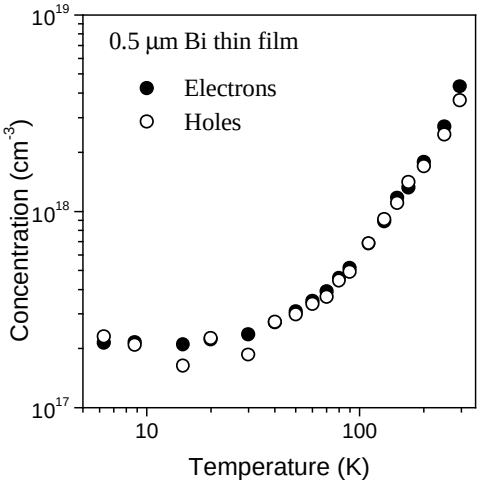

Figure 1. Electron (filled points) and hole (open points) densities as a function of temperature for the 0.5 μm Bi thin film, as determined from analysis of the Hall data with the anisotropic QMSA procedure.

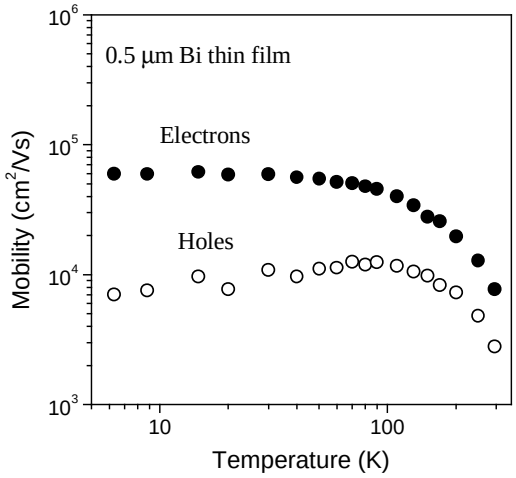

Figure 2. Average electron (filled points) and hole (open points) mobilities as a function of temperature for the 0.5 μm Bi thin film from application of the anisotropic QMSA procedure to the Hall data.

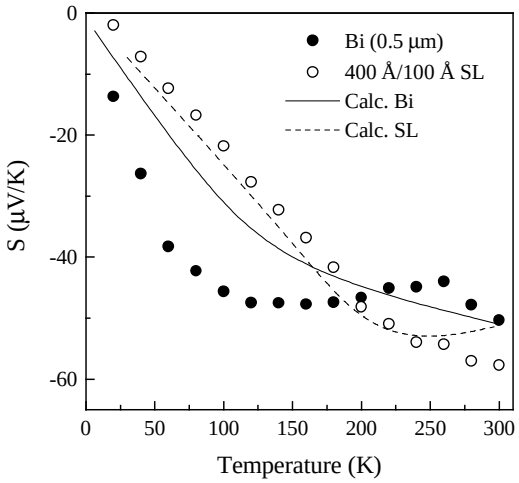

Figure 3. Experimental (points) and theoretical (curves) thermoelectric powers for the 0.5 μm Bi thin film and the nine-period 400 Å/100 Å Bi/CdTe superlattice.

carrier-statistical calculations described above. At $T = 6.3$ K, the average electron mobility is found to be 6.4×10^4 cm^2 V^{-1} s^{-1} and the hole mobility is 6600 cm^2 V^{-1} s^{-1}, whereas nearly equal electron and hole mobilities are obtained if the electrons are taken to be isotropic [8].

Thermopowers were calculated from equations (4) and (5), using the QMSA densities to derive the Fermi energies and the QMSA mobilities to fix the normalization of the momentum relaxation times. The result is given by the solid curve of figure 3, which is in good agreement with the experimental data represented by the filled points, when it is considered that the model incorporating input from the transport measurements contains no adjustable parameters. The relatively modest discrepancy at lower temperatures is probably due to a slight underestimate of the electron-to-hole mobility ratio obtained from the magnetotransport characterization.

5.2. Bi/CdTe superlattices

Similar analyses were carried out on data from the two Bi/CdTe superlattice samples. The band parameters for the Bi well layer were taken to be identical to those in the bulk, since the well thicknesses were too large to produce any appreciable quantum confinement effects. Because the superlattices were unintentionally doped n-type to approximately 1×10^{19} cm^{-3}, intrinsic generation becomes pronounced only at higher temperatures.

Experimental and theoretical thermopower results for the 400 Å/100 Å superlattice are indicated by the open points and dashed curve, respectively, in figure 3. In this case, the agreement is even better than for the Bi thin film, probably because $n \gg p$, and hence the mobility ratio is not as critical. While at low temperatures the magnitude of the thermopower is smaller than that for the Bi thin film (due to the much stronger degeneracy of the electrons), S increases rapidly with T as the degeneracy is reduced. At high temperatures, the thermopower exceeds that in the Bi film owing to a smaller hole population even though the mobility ratio is closer to unity than in Bi. The agreement between the theoretical and experimental results for the 800 Å/100 Å superlattice is quite similar.

5.3. $Bi_{1-x}Sb_x$ alloy thin films

In analysing the transport data for the two $Bi_{1-x}Sb_x$ samples, a larger mobility ratio of 250 was assumed [25]. As was discussed above, the data were insufficiently sensitive for the QMSA procedure to be used with no constraining conditions. Therefore, we performed a standard multicarrier fit including anisotropy and assuming the presence of three carrier species: electrons in the L_a valley, holes in the T valley, and holes in the L_s valley. The fit was made subject to the following constraints. First, the difference between the electron and hole densities $n - p$ was fixed at its low-temperature value, which represents the net donor concentration (4×10^{16} cm^{-3} for $x = 0.09$), since $p = 0$ at low T in these semiconducting alloys. Second, in the multicarrier fitting procedure, fractions of the total hole population residing in the T and L valleys, computed as a function of temperature with the aid of the statistical model described above, were fixed. Since the temperature dependence of the energy gap in $Bi_{1-x}Sb_x$ has apparently not been measured, we used the relation for the L-valley gap in Bi [26]. We also took the value of the T-valley direct gap to be 0.41 eV as previously determined from magnetotransmission measurements [27]. The model yields that for $x = 0.09$ and $T = 80$ K, 79% of all holes should be in the T valley, which has a considerably larger density of states near the band edge than the L valleys. However, the L-valley density of states increases rapidly away from the band edge owing to the strong nonparabolicity, and, at room temperature, the holes are predicted to be split almost evenly between the two valleys. The multicarrier transport analysis was then carried out in the following two limits: (1) both L- and T-valley hole mobilities were allowed to float; (2) the L-valley mobility was allowed to float, but the T-valley mobility was set to be equal to the value obtained for the pure Bi film at the same temperature. The latter approximation seems reasonable insofar as the T-valley mass is not expected to have a strong dependence on alloy concentration, and intervalley electron–hole scattering, which is present in Bi but not in the semiconducting alloy, is not expected to be a dominant relaxation mechanism. As a consequence, the hole mobility should not differ greatly from its value in Bi. In order to test the sensitivity of the multicarrier fit and the thermopower to the value assumed for the indirect energy gap (between the L_a and T valleys), calculations were carried out for a range of ε_g in addition to the literature value of 12 meV (taken to be independent of temperature).

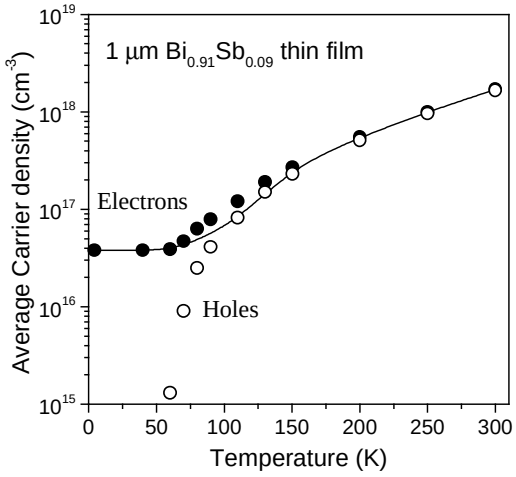

Figure 4. Electron concentration (averaged over the total thickness, filled circles), net hole concentration (open circles) from the multicarrier fit to the magnetotransport data for the $Bi_{0.91}Sb_{0.09}$ film. Also shown is the carrier-statistical calculation of the electron density obtained assuming a gap of 12 meV (curve).

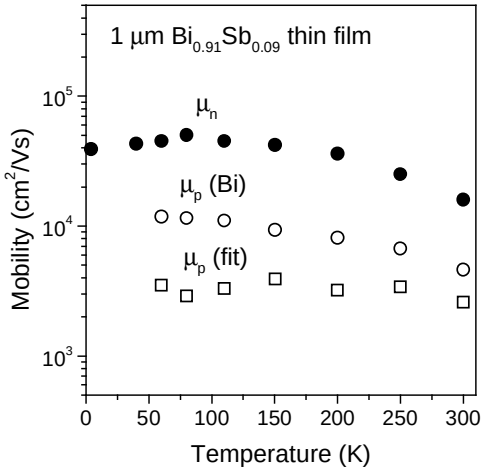

Figure 5. Electron mobility (filled circles), hole mobility, averaged over L- and T-valley contributions, with floating mobilities for both species (open circles) and average hole mobility when the T-valley mobility is fixed at its value for Bi (open boxes) as a function of temperature for the 1 μm $Bi_{0.91}Sb_{0.09}$ thin film. For anisotropic carriers, the average value for the mobility is always shown.

Results for the electron concentration (filled circles) and net hole concentration (both L and T valleys, open circles) in this film are shown in figure 4. Corresponding fits for the electron mobility (filled circles), average hole mobility when the values for both hole species are allowed to float (open circles) and average hole mobility when μ_{pT} is fixed at the value for Bi (open boxes) are given in figure 5. For anisotropic carriers, the *average* mobility value is always shown. The two hole mobilities are seen to differ by a factor of two to three. The curve in figure 4 is from a statistical calculation of the electron density, in which the electron and hole effective masses near the band edges have been adjusted from their literature values

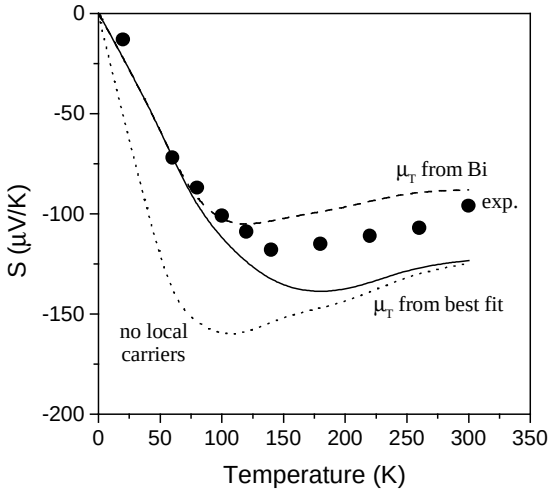

Figure 6. Experimental (points) and theoretical (curves) thermopowers as a function of temperature for the 1 μm $Bi_{0.91}Sb_{0.09}$ thin film. The solid curve corresponds to a floating T-valley mobility, whereas the dashed curve demonstrates the results of assuming the T-valley mobility equal to that in the Bi thin film. The thermopower resulting from assuming no local carriers and a floating T-valley mobility is shown by the dotted curve.

by a constant multiplicative factor of 1.2. This is done in order to fit the experimental room-temperature density of $n = 1.7 \times 10^{18}$ cm^{-3}, which is in good agreement with previous determinations [1]. Note that the model then reproduces the experimental dependence $n(T)$ quite well. For the temperature range of 60–100 K, in which thermally excited intrinsic carriers begin to appear, slightly better agreement is obtained by using a gap smaller than 12 meV, and somewhat worse when a larger indirect gap (e.g., 35 meV) is assumed. Whereas fits to intrinsic carrier concentrations obtained from multicarrier analyses often offer a valuable tool for characterizing energy gaps in narrow-gap semiconductors [28], here the sensitivity of $n_i(T)$ to ε_g is somewhat reduced due to the extreme nonparabolicity of the bands when the gap goes to zero. According to equation (3), the electron and hole dispersions become linear and independent of ε_g when $\varepsilon(k) \gg \varepsilon_g$.

Figure 6 compares the experimental (points) and theoretical (curves) thermopowers for the $Bi_{0.91}Sb_{0.09}$ film. If the calculation employs the density and mobility values given in figure 4, the theoretical thermopower represented by the dotted curve in figure 6 significantly exceeds the measured values at low temperatures. The discrepancy must be in the description of the electrons, since few holes are present at temperatures below 100 K. The most obvious way to improve the agreement is to increase electron degeneracy, for example, by decreasing the electron mass. However, it is physically unreasonable to suppose that the mass tensor components employed in the calculation are larger by the necessary amount. Owing to the strong nonparabolicity, even reducing the energy gap to zero does not decrease the mass enough to appreciably improve the agreement with experiment. The alternative is to conclude that the electron density employed in the calculation is too small (at low temperatures). This does not necessarily contradict the findings of the magnetotransport data, since that experiment yields only a net sheet concentration present in the plane of the current flow, without providing information about the density profile of those carriers along the growth axis. In fact, previous studies of Bi-based thin films observed a carrier component whose concentration did not scale with film thickness [2, 29]. This component presumably results from interface defects and,

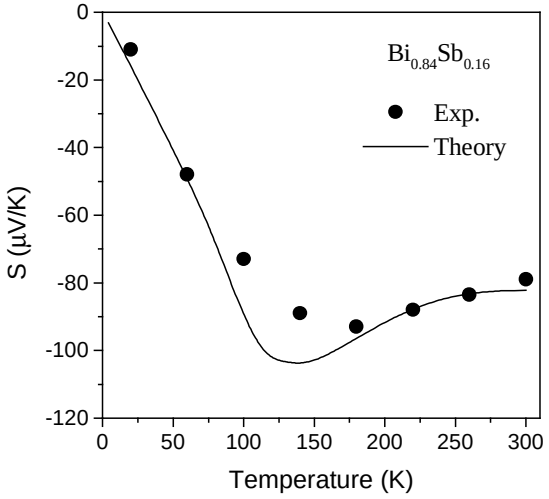

Figure 7. Experimental (points) and theoretical (solid curve) thermopowers as a function of temperature for the 1 μm $Bi_{0.84}Sb_{0.16}$ thin film.

due to band bending, tends to be localized in the vicinity of the interface. The solid and dashed curves of figure 6 (corresponding to the two assumptions about hole mobility) represent the results of assuming that the electrons observed at low temperatures are concentrated with a sheet density of $N_I = 4 \times 10^{12}$ cm^{-2} (intermediate between the values reported in [2] and [29]) over a thickness of 2000 Å rather than over the total film thickness of 1 μm. With this assumption, the local electron density is $\approx 2 \times 10^{17}$ cm^{-3}, and the degeneracy is great enough to account for the experimental thermopower at low T. As the temperature increases to the point where additional electrons and holes are thermally excited, those carriers are expected to spread out uniformly through the entire film. The dashed and solid curves, which account for both localized and bulk carriers and take the energy gap to be 12 meV, are seen to bracket the measured values. If the same procedure is followed while assuming a larger energy gap of 35 meV, the agreement between theory and experiment is not as good at intermediate temperatures. However, as for the intrinsic carrier concentration (figure 4), the difference is not great enough to represent a definitive argument against a larger value for ε_g.

For $Bi_{0.84}Sb_{0.16}$, the conduction band minimum again occurs in the L_a valley. However, the H valley moves up in energy with increasing x, so that at $x = 0.16$ the H and L_s valence band maxima are at approximately the same energy (with the T-valley maximum somewhat lower). Since the H valley is sixfold degenerate and has a much larger density of states than L_s, even at room temperature up to 90% of the holes are believed to reside in the H valley. Unfortunately, there appear to be no published characterization studies reporting the properties of H-valley holes in Bi-rich $Bi_{1-x}Sb_x$ alloys. For lack of better information, we therefore take the H-valley direct bandgap, hole masses near the band edge and mobility anisotropy ratio ($\approx$20) in the $Bi_{0.84}Sb_{0.16}$ thin film to be equal to those in bulk Sb [16, 30].

The procedure outlined above for $Bi_{0.91}Sb_{0.09}$ was followed again to analyse the magnetotransport and thermopower data for $Bi_{0.84}Sb_{0.16}$. An anisotropic multicarrier fit yielded an *average* electron density of 3.5×10^{17} cm^{-3} at 60 K, which corresponds to a local density of $\approx 7 \times 10^{17}$ cm^{-3} when the interface localization is taken into account. The H-valley hole mobility in the fit was constrained to have an upper bound equal to 10% of the L-valley electron mobility (consistent with previous experiments for this x range), whereas the L-valley hole

mobility was allowed to float. At room temperature, the electron density of 3.5×10^{18} cm^{-3} is larger than that in $Bi_{0.91}Sb_{0.09}$, which reflects the larger valence band density of states in the $x = 0.16$ alloy.

Figure 7 shows the experimental (points) and theoretical (curves) results for the thermopower as a function of temperature in the $Bi_{0.84}Sb_{0.16}$ thin film, for which an indirect energy gap was assumed to have its bulk value of 30 meV. The increased (non-uniform) carrier density and hence greater electron degeneracy forces theory and experiment to agree at low temperatures. The agreement at high temperatures is also quite good, although the magnitude of S from the theory is somewhat too large at intermediate temperatures. The calculated results are again relatively insensitive to variations of the energy gap.

6. Conclusions

We have studied the thermoelectric properties of BiSb thin films and Bi/CdTe superlattices. The thermopower has been calculated using a band structure, statistical and transport model that incorporates electron and hole densities and mobilities derived from field-dependent Hall and resistivity measurements that were analysed by the anisotropic QMSA and multicarrier fitting approaches. For a Bi thin film and two Bi/CdTe superlattices, the model achieves good agreement with experimental thermopowers with no adjustable parameters. However, the low-temperature thermopowers for $Bi_{1-x}Sb_x$ alloy thin films with $x = 0.09$ and $x = 0.16$ can only be accounted for by assuming that the electrons associated with net donors are localized in the region adjacent to the substrate (these are associated with interface defects, but still available for conduction) rather than being distributed uniformly throughout the 1 μm total film thickness. On the other hand, in Bi/CdTe superlattices with well thicknesses $\leqslant$800 Å, each well is thinner than the region over which band bending localizes the carriers, and the electrons are distributed more or less uniformly over the entire width of the well.

Acknowledgments

Work at Northwestern University and NRL was supported in part by DARPA under grant No DAAG55-97-1-130 and the anisotropic QMSA work at NRL was also supported by a CRDA with LakeShore Cryotronics, Inc.

References

[1] Heremans J, Partin D L, Thrush C M, Karczewski G, Richardson M S and Furdyna J K *Phys. Rev.* B **48** 11 329
[2] Hoffman C A, Meyer J R, Bartoli F J, DiVenere A , Yi X J, Hou C L, Wang H C, Ketterson J B and Wong G K 1993 *Phys. Rev.* B **48** 1143
Hoffman C A, Meyer J R, Bartoli F J, DiVenere A , Yi X J, Hou C L, Wang H C, Ketterson J B and Wong G K 1995 *Phys. Rev.* B **51** 5535
[3] Cho S, DiVenere A, Wong G K, Ketterson J B, Meyer J R and Hoffman C A 1997 *Solid State Commun.* **102** 673
[4] Lenoir B, Cassart M, Michenaud J-P, Scherrer H and Scherrer S 1996 *J. Phys. Chem. Solids* **57** 89
[5] Hicks L D and Dresselhaus M S 1993 *Phys. Rev.* B **47** 12 727
[6] Broido D A and Reinecke T L 1995 *Phys. Rev.* B **51** 13 797
[7] Gallo C F, Chandrasekhar B S and Sutter P H 1963 *J. Appl. Phys.* **34** 144
[8] Vurgaftman I, Meyer J R, Hoffman C A, Cho S, Ketterson J B, Faraone L, Antoszewski J and Lindemuth J R 1999 *J. Electron. Mater.* **28** 548
[9] DiVenere A *et al* 1994 *J. Vac. Sci. Technol.* B **12** 1136
[10] Cho S, DiVenere A, Wong G K, Ketterson J B and Meyer J R 1999 *J. Appl. Phys.* **85** 3655
[11] Antoszewski J, Seymour D J, Faraone L, Meyer J R and Hoffman C A 1995 *J. Electron. Mater.* **24** 1255
[12] Meyer J R, Hoffman C A, Antoszewski J and Faraone L 1997 *J. Appl. Phys.* **81** 709

[13] Vurgaftman I, Meyer J R, Hoffman C A, Redfern D, Antoszewski J, Faraone L and Lindemuth J R 1998 *J. Appl. Phys.* **84** 4966
[14] van Hulst J A, Jaeger H M and Radelaar S 1995 *Phys. Rev.* B **52** 5953
[15] Beck W A and Anderson J R 1987 *J. Appl. Phys.* **62** 541
[16] For a review of group-V semimetals, see J-P Issi 1979 *Aust. J. Phys.* **32** 585
[17] Nemchinskii V A and Ravich Yu I 1991 *Fiz. Tverd. Tela* **33** 2071 (Engl. Transl. *Sov. Phys.–Solid State* **33** 1165 (1991))
[18] Ravich Yu I and Rapoport A V 1992 *Fiz. Tverd. Tela* **34** 1801 (Engl. Transl. 1992 *Sov. Phys.–Solid State* **34** 960)
[19] Price P J 1960 *IBM J.* April 152
[20] Seeger K 1973 *Semiconductor Physics* (New York: Springer) p 93
[21] Meyer J R, Hoffman C A, Bartoli F J, Arnold D A, Sivananthan S and Faurie J P 1993 *Semicond. Sci. Technol.* **8** 805
[22] Saunders G A and Sümengen Z 1972 *J. Phys. F: Met. Phys.* **2** 972
[23] Abeles B and Meiboom S 1956 *Phys. Rev.* **101** 544
[24] Michenaud J-P and Issi J-P 1972 *J. Phys. C: Solid State Phys.* **5** 3061
Mikhail I F I, Hansen O P and Nielsen H 1980 *J. Phys. C: Solid State Phys.* **13** 1697
[25] Yazaki T and Abe Y 1968 *J. Phys. Soc. Japan* **24** 290
[26] Vecchi M P and Dresselhaus M S 1974 *Phys. Rev.* B **10** 771
[27] Omaggio J P *et al* 1993 *Phys. Rev.* B **48** 11 439
[28] Omaggio J P *et al* 1992 *Appl. Phys. Lett.* **61** 207
[29] Komnik Yu F, Bukhshtab E I, Nikitin Yu V and Andrievskii V V 1971 *Zh. Eksp. Teor. Fiz.* **60** 669 (Engl. Transl. 1971 *Sov. Phys.–JETP* **33** 364)
[30] Bresler M S and Red'ko N A 1972 *Zh. Eksp. Teor. Fiz.* **61** 287 (Engl. Transl. 1971 *Sov. Phys.–JETP* **34** 149)
[31] Isaacson R T and Williams G A 1969 *Phys. Rev.* **185** 682